TOPICAL REVIEW — Statistical physics and complex systems

Level spacing statistics for two-dimensional massless Dirac billiards*

Huang Liang(黄 亮)[a)b)†], Xu Hong-Ya(徐洪亚)[a)b)], Lai Ying-Cheng(来颖诚)[b)c)d)], and Celso Grebogi[d)]

[a)]*Institute of Computational Physics and Complex Systems and Key Laboratory for Magnetism and Magnetic Materials of MOE, Lanzhou University, Lanzhou 730000, China*

[b)]*School of Electrical, Computer, and Energy Engineering, Arizona State University, Tempe, AZ 85287, USA*

[c)]*Department of Physics, Arizona State University, Tempe, AZ 85287, USA*

[d)]*Institute for Complex Systems and Mathematical Biology, School of Natural and Computing Sciences, King's College, University of Aberdeen, UK*

Classical-quantum correspondence has been an intriguing issue ever since quantum theory was proposed. The searching for signatures of classically nonintegrable dynamics in quantum systems comprises the interesting field of quantum chaos. In this short review, we shall go over recent efforts of extending the understanding of quantum chaos to relativistic cases. We shall focus on the level spacing statistics for two-dimensional massless Dirac billiards, i.e., particles confined in a closed region. We shall discuss the works for both the particle described by the massless Dirac equation (or Weyl equation) and the quasiparticle from graphene. Although the equations are the same, the boundary conditions are typically different, rendering distinct level spacing statistics.

Keywords: quantum chaos, level spacing statistics, Dirac billiards, graphene billiards

1. Introduction

In the last three decades, quantum chaos, an interdisciplinary field focusing on the quantum manifestations of classical chaos, has received a great deal of attention from a number of physics communities.[1–3] Indeed, the quantization of chaotic Hamiltonian systems and signatures of classical chaos in quantum regimes are fundamental in physics and are directly relevant to fields such as condensed matter physics, atomic physics, nuclear physics, optics, and acoustics.[1–3] Issues that have been pursued include energy-level statistics, statistical properties of wave functions, quantum chaotic scattering, electronic transport in quantum dots, localization, and the effects of magnetic fields, etc. A fundamental result in non-relativistic quantum nonlinear dynamics is that, for systems without geometrical symmetries and whose classical dynamics are chaotic, their energy level-statistics are described by those of random matrices.[2–8] In particular, if the system possesses time-reversal symmetry, there will be a representation that the Hamiltonian matrix is real symmetric. This property is preserved under orthogonal transformations, and the resulting energy level-spacing statistics (LSS) will follow the distribution of those of random matrices from the Gaussian orthogonal ensemble (GOE).[1] If, in addition to time-reversal symmetry, the system has a half-integer spin interaction, then the Hamiltonian can be represented by quaternion real matrices which are invariant under symplectic transformations. As a consequence, the resulting level-spacing statistics follow those of random matrices from the Gaussian symplectic ensemble (GSE). When the time-reversal symmetry is broken, e.g., as in the presence of a magnetic field, the system is invariant under the unitary transformations, and the level-spacing statistics are governed by the Gaussian unitary ensemble (GUE) random matrices. Both the GOE and GUE statistics have been observed experimentally for non-relativistic quantum (wave) systems exhibiting chaotic dynamics in the classical limit.[1,9,10]

In the vast literature, most existing works on quantum chaos are concerned exclusively with non-relativistic quantum mechanical systems described by the Schrödinger equation, where the dependence of particle energy on momentum is quadratic. A natural question is whether the phenomena in non-relativistic quantum nonlinear dynamics can occur in relativistic quantum systems. This is important, as whether the classical dynamics plays a role in the relativistic quantum systems is fundamental, and this is a nontrivial extension as it has features such as intrinsic spin, linear dispersion relation, Klein tunneling, and chirality, etc., that are not shared by the nonrelativistic quantum physics. Here in this manuscript we shall specifically focus on massless two-dimensional (2D) (pseudo-) Dirac fermions described by the 2D Dirac equation with zero mass, where the energy–momentum relation is linear. To ask this question may appear conceptually interesting but may not have realistic physical correspondence before the past decades, especially for the billiard models.

http://iopscience.iop.org/cpb   http://cpb.iphy.ac.cn

This is because, from an experimental point of view, a relativistic particle cannot be confined within a designed region due to the Klein tunneling effect, say, the Dirac billiard, in contrast to the non-relativistic electron case. However, in the last decade, the great progress in graphene[11–14] and topological insulator[15–17] has made it convenient to simulate a relativistic Dirac billiard via the quasiparticles of the electrons in graphene or topological insulators. This has led to a boom of theoretical investigations on relativistic quantum chaos, i.e., to study the behavior of relativistic quantum systems with classically chaotic dynamics,[19–25] and also makes it an appealing topic due to the possibility of experimental verification.[26–30]

In relativistic quantum mechanics, the seminal work of Berry and Mondragon[31] established that, for massless spin-half particles such as neutrinos[32] in a 2D billiard model, if the classical dynamics are integrable, the level-spacing statistics are Poissonian, which are similar to those in integrable non-relativistic quantum systems. However, when the classical dynamics are chaotic, the level-spacing distributions are persistently those of GUE, even in the absence of any magnetic field. This is due to the chiral nature of Dirac particles and the confinement scalar potential that breaks the time-reversal symmetry. Since its prediction over two decades ago,[31] this phenomenon has not been tested experimentally, partly due to the difficulty of constructing relativistic quantum systems with chaotic classical dynamics in the laboratory. Note that this anomaly is absent for the three-dimensional Dirac billiards.[33]

Recently, graphene, a single, one-atom-thick sheet of carbon atoms arranged in a honeycomb lattice, has been realized in experiments.[34] In the low-energy regime, quasiparticle motions in graphene are characteristic of those of relativistic, massless Dirac fermions and, consequently, devices made of graphene are potentially capable of operating at a much higher speed than those based on conventional silicon electronics.[26,27] Graphene confinements that have the geometric shape of chaotic billiards thus represent a potential experimental system for testing energy-level statistics in the relativistic quantum regime. There have been considerable efforts investigating the level spacing statistics for graphene billiards (flakes) aiming to uncover the results of Berry and Mondragon.[31]

In this short review, we shall go over the works of the level spacing statistics for both graphene billiards (that represent confined pseudo-Dirac particles) and 2D Dirac billiards by solving the massless Dirac equations. Note that the two are different. For graphene, only the pseudo-particles around one Dirac point follow the same massless Dirac equations. The boundary conditions are different from that of the Dirac billiards. Although for open graphene systems, electrons belonging to the two valleys can be separated,[35–37] for closed graphene billiards, the two valleys are usually coupled by the

scattering at the boundary; therefore, the observed phenomena are for two coupled Dirac fermions within the billiard region. Thus graphene systems can have properties that are not shared by either non-relativistic quantum or purely relativistic quantum systems. The distribution of energy levels may have implications for graphene-based devices that use quantum dots,[26–30] a kind of "open" billiard structure.

1.1. Quantities to be calculated for level spacing statistics

Once the energy spectra in the interested region is obtained, it can be unfolded to get the unfolded spectra: $x_n \equiv \langle N(E_n) \rangle$. Let $S_n = x_{n+1} - x_n$ be the nearest-neighbor spacing and $P(S)$ be the distribution function of S_n, it can be verified that $\int S P(S) \, \mathrm{d}S = 1$. For non-relativistic quantum billiards, the distribution of this unfolded level-spacing follows several universal classes, depending on the nature of the corresponding classical dynamics and symmetry. In particular, if classically the system is integrable, the distribution is Poissonian:[38]

$$P(S) = \mathrm{e}^{-S}. \tag{1}$$

For quantum billiards that are completely chaotic in the classical limit and do not possess any geometric symmetry,[39,40] the level-spacing distributions follow the GOE statistics if the system has time-reversal symmetry[41]

$$P(S) = \frac{\pi}{2} S \mathrm{e}^{-\pi S^2/4}, \tag{2}$$

and GUE statistics if the system has no time-reversal symmetry

$$P(S) = \frac{32}{\pi} S^2 \mathrm{e}^{-(4/\pi)S^2}. \tag{3}$$

The cumulative level-spacing distribution can then be obtained by

$$I(S) = \int_0^S P(S') \mathrm{d}S'. \tag{4}$$

Another index for the universal classes is the spectral rigidity $\Delta_3(L)$, which is used to measure long-range spectral fluctuations and is defined as[42]

$$\Delta_3(L) = \left\langle \min(a,b) L^{-1} \int_{-L/2}^{L/2} \mathrm{d}x \{ N(x_0 + x) - ax - b \}^2 \right\rangle, \tag{5}$$

where the average is over x_0. Numerically, if n unfolded levels $\widetilde{x}_i = x_i - x_0$ lie in the interval $[-L, L]$, e.g., $-L \leq \widetilde{x}_1 \leq \cdots \leq \widetilde{x}_n \leq L$, the integral in the above equation yields[43]

$$\begin{aligned}
\Delta_3(2L, x_0) = {} & \frac{n^2}{16} - \frac{1}{4L^2} \left[\sum_{i=1}^n \widetilde{x}_i \right]^2 \\
& + \frac{3n}{8L^2} \left[\sum_{i=1}^n \widetilde{x}_i^2 \right] - \frac{3}{16L^4} \left[\sum_{i=1}^n \widetilde{x}_i^2 \right]^2 \\
& + \frac{1}{2L} \left[\sum_{i=1}^n (n - 2i + 1) \widetilde{x}_i \right],
\end{aligned} \tag{6}$$

and $\Delta_3(L) = \langle \Delta_3(L, x_0) \rangle_{x_0}$. Theoretically, $\Delta_3(L)$ for a correlated unfolded energy-level sequence is given by

$$\Delta_3(L) = \frac{1}{15L^4}\left[L^5 - \int_0^L du(L-u)^3 \right.$$
$$\left. \times (2L^2 - 9Lu - 3u^2)Y(u) \right], \qquad (7)$$

where $Y(u)$ is the following two-level cluster function:[44]

$$Y(u) = 0, \qquad \text{for Poisson,}$$
$$Y(u) = U(u)^2 + \frac{d}{du}U(u) \times \int_u^\infty dt\, U(t), \ \text{ for GOE,}$$
$$Y(u) = U(u)^2, \qquad \text{for GUE,}$$

and $U(u) = \sin(\pi u)/(\pi u)$.

Phenomenologically, Hasegawa proposed a function to bridge the Poisson distribution and the GOE distribution[45]

$$P_H(S;\alpha,\beta) = N\frac{\rho S\, \mathrm{e}^{-\rho S - (\alpha\rho S)^2/2}}{\sqrt{\rho^2 S^2\, \mathrm{e}^{-(\alpha\rho S)^2} + \beta^2\, \mathrm{e}^{-2\rho S}}}, \qquad (8)$$

where ρ and N are determined by the normalization conditions $\int P_H\, dS = \int S P_H\, dS = 1$. The control parameter β describes the transition from Poissonian $\beta = 0$ to GOE statistics $\beta \to \infty$, α is a system-specific constant.

2. Berry's neutrino billiards

Berry and Mondragon[31] considered a confined neutrino[32] model and calculated the eigenenergies. To be specific, consider a massless spin-half particle in a finite domain D in the plane $\mathbf{r} = (x, y)$. Utilizing an infinite-mass term outside the domain to model the confinement of the particle motion within D, the Hamiltonian in the position representation is given by

$$\hat{H} = -\mathrm{i}\hbar v\hat{\boldsymbol{\sigma}} \cdot \boldsymbol{\nabla} + V(\mathbf{r})\hat{\sigma}_z, \qquad (9)$$

where $\hat{\boldsymbol{\sigma}} = (\hat{\sigma}_x, \hat{\sigma}_y)$ and $\hat{\sigma}_z$ are Pauli matrices, and $V(\mathbf{r})$ is the infinite-mass confinement potential

$$V(\mathbf{r}) = \begin{cases} 0, & \mathbf{r} \in D, \\ \infty, & \mathbf{r} \text{ outside of } D. \end{cases} \qquad (10)$$

The Hamiltonian $\hat{H}$ acts on two-component spinor wave-function $\boldsymbol{\psi}(\mathbf{r}) = [\psi_1, \psi_2]^{\mathrm{T}}$ and it has eigenenergy E, i.e.,

$$[-\mathrm{i}\hbar v\hat{\boldsymbol{\sigma}} \cdot \boldsymbol{\nabla} + V(\mathbf{r})\hat{\sigma}_z]\boldsymbol{\psi}(\mathbf{r}) = E\boldsymbol{\psi}(\mathbf{r}). \qquad (11)$$

Some basic properties of Eq. (11) are the following. First, the confinement condition of imposing infinite mass outside D naturally overcomes the difficulty for electric potential due to the Klein paradox for relativistic quantum particles. Second, the reduced spatial dimension and confinement break the time-reversal symmetry of $\hat{H}$, namely

$$[\hat{T}, \hat{H}] \neq 0, \qquad (12)$$

where $\hat{T} = \mathrm{i}\sigma_y\hat{K}$, and $\hat{K}$ denotes the complex conjugate. Third, for $V = 0$ in Eq. (11), there exist plane-wave solutions whose positive-energy part has the following form:

$$\boldsymbol{\psi}_{\mathbf{k}}(\mathbf{r}) = \frac{1}{\sqrt{2}} \begin{pmatrix} \exp\left(-\mathrm{i}\dfrac{\theta}{2}\right) \\[2mm] \exp\left(\mathrm{i}\dfrac{\theta}{2}\right) \end{pmatrix} \exp(\mathrm{i}\mathbf{k} \cdot r), \qquad (13)$$

where $\mathbf{k}$ is a wave-vector that makes an angle θ with the x axis.

To obtain solutions of Eq. (11), a proper treatment of the boundary condition is necessary. As shown in Fig. 1, let the outward normal unit at s be $\mathbf{n}(s) = [\cos(\alpha), \sin(\alpha)]$. Making use of the hermiticity of $\hat{H}$ and defining $\mathbf{j} = c\psi^\dagger\hat{\boldsymbol{\sigma}}\psi$ as the local relativistic current, one gets the vanishing current condition: $\mathbf{j} \cdot n = 0$ for any point s. Requiring the outward current to be zero cannot fix the boundary condition uniquely but it entails $\mathrm{Re}(\exp(\mathrm{i}\alpha)\psi_1/\psi_2) = 0$ for each point s. Using the boundary potential (10), the complete boundary condition can be finally determined as[31]

$$\frac{\psi_2}{\psi_1} = \mathrm{i}\exp[\mathrm{i}\alpha(s)]. \qquad (14)$$
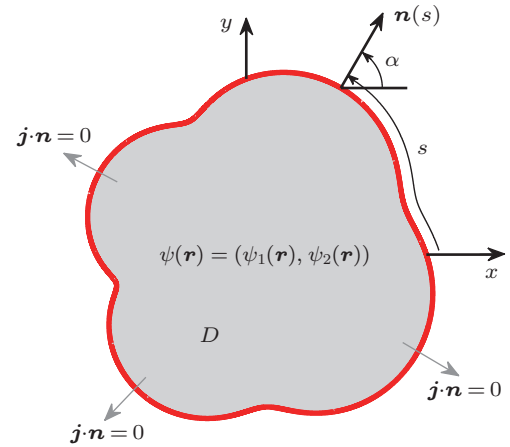
Fig. 1. Illustration of a chaotic domain with boundary parameterized by arc length s. For the motion of a massless Dirac fermion inside the domain, the boundary condition is of the zero-flux type, i.e., no outward current at any point s: $\mathbf{j} \cdot n = 0$.

Berry and Mondragon[31] implemented the boundary integral method to calculate the eigenenergies for this billiard system. In their paper, they considered two shapes, the unit circle with integrable classical dynamics (left columns of Fig. 2) and the Africa billiard (middle columns of Fig. 2) with the boundary given by

$$w(z) = (z + 0.2z^2 + 0.2z^3\, \mathrm{e}^{\mathrm{i}\pi/3}),$$

whose classical motions are chaotic. Here, z belongs to the unit circle. Note that this Africa billiard has no mirror or other discrete symmetries. Here we shall also consider a heart

shaped billiard (right columns of Fig. 2), where the boundary is given by a conformal mapping from the unit circle

$$w(z) = \frac{1}{\sqrt{1+2\beta^2}}(z+\beta z^2), \quad \beta \in [0, \frac{1}{2}),$$

for $\beta = 0.49$, a previous work on the classical dynamics of the billiard[46] demonstrated the presence of chaos. The heart shaped billiard has an up-down mirror symmetry.

For non-relativistic billiards, according to the Weyl formula,[1,3] the smoothed wave-vector staircase function is given by

$$\langle \mathcal{N}(k) \rangle = \frac{\mathcal{A}k^2}{4\pi} + \gamma \frac{\mathcal{L}k}{4\pi} + \cdots, \tag{15}$$

where $\mathcal{A}$ and $\mathcal{L}$ are the area and perimeter of the billiard, respectively, $\gamma = -1$ (or 1) for Dirichlet (or Neumann) boundary conditions. While for the neutrino billiard, Berry and Mondragon have shown that $\gamma = 0$,[31] so there is no perimeter correction.

For better visualization, we have recalculated the eigenenergies by a conformal mapping method,[21] which can calculate the eigenstates simultaneously with the eigenenergies, also with a better accuracy. For the above three cases, we have calculated 13000 energy levels each, and the results are shown in Fig. 2.
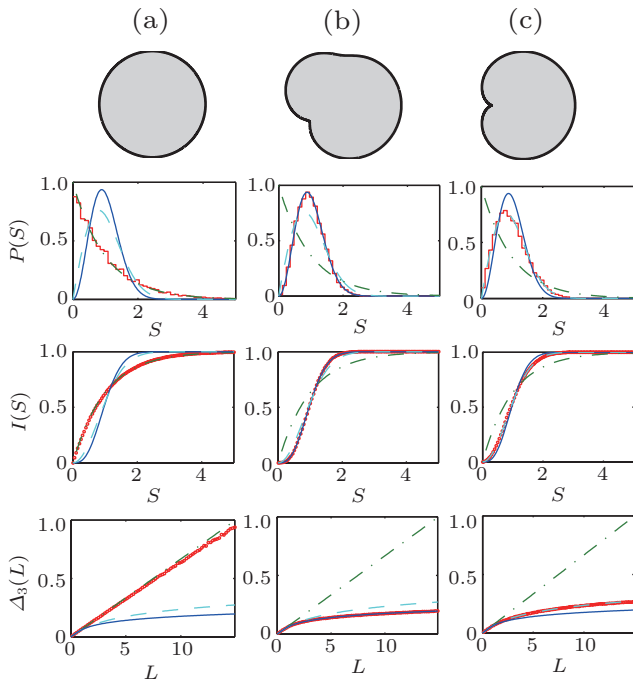
Fig. 2. Level spacing statistics of neutrino billiards. (a) Circle; (b) Africa billiard; (c) heart shaped billiard. The first row shows the shape of the billiards. The second to the fourth rows are the unfolded level-spacing distribution $P(S)$, the cumulative level-spacing distribution $I(S)$, and the spectral rigidity $\Delta_3(L)$, respectively. The green dash-dotted line, cyan dashed line, and blue solid line are for Poisson, GOE, and GUE, respectively. Red symbols are numerical results from 13000 energy levels for each shape.

From the various quantities plotted, the statistics is Poisson for the integrable case, while for the chaotic Africa bil-

liard where the shape has no geometric symmetry, the resulting level spacing distribution is GUE, as the time reversal symmetry is broken. For the heart shaped billiard, since it has a mirror symmetry, it is invariant under the combination of time-reversal and reflection operations, which leads to GOE.

Ni *et al.*[47–49] developed a direct discretization method to solve the spectrum and eigenstates of a massless Dirac billiard in any infinite-mass confinement with any electric potentials, i.e., a potential barrier. They have also repeated the above results by Berry and Mondragon.

3. Graphene billiards

3.1. Basics of graphene billiards

For a graphene confinement, the tight-binding Hamiltonian is given by

$$\hat{H} = \sum(-\varepsilon_i)|i\rangle\langle i| + \sum(-t_{ij})|i\rangle\langle j|, \tag{16}$$

where the first summation is over all the atoms and the second summation is over all pairs of all necessary neighboring atoms, which should include the nearest neighboring pairs, but may also include the next or next-next nearest neighboring pairs, with their respective hopping energy t_{ij}'s according to the distance or whether the atoms are located at the boundary. For clean graphene, the onsite energy ε_i is identical for all atoms and only contributes to a shift in the energy spectrum, thus it is often omitted. While in the presence of disorders, the distortion potential is usually applied to the onsite energy.

In the presence of a magnetic field, the hopping energy will be modified with a phase factor:

$$\widetilde{t}_{ij} = t_{ij}\exp(-i\frac{2\pi}{\phi_0}\int_{\boldsymbol{r}_j}^{\boldsymbol{r}_i} d\boldsymbol{r}\cdot\boldsymbol{A}), \tag{17}$$

where $\boldsymbol{A}$ is the vector potential associated with the magnetic field, and $\phi_0 = h/e = 4.136 \times 10^{-15}$ T·m^2 is the magnetic flux quantum. Using the Landau gauge, the vector potential is given by $\boldsymbol{A} = (-By, 0, 0)$ for a perpendicular uniform magnetic field B pointing out the billiard plane. For convenience, the magnetic flux $\phi = BS$ through a hexagonal plaque is used as a parameter characterizing the magnetic field, where the area is $S = 3\sqrt{3}/2a_0^2 = 5.24$ Å^2, and $a_0 = 1.42$ Å is the atom separation of the graphene lattice. The eigenenergies can then be calculated by diagonalizing the tight-binding Hamiltonian matrix.

In order to address the relativistic quantum nature of the quasiparticle motions in graphene, in the studies of level spacing statistics, one usually focuses on the energy levels around the Dirac points. Particularly, figure 3 shows the energy-wavevector relation for an infinite graphene lattice in the absence of a magnetic field. As can be seen from the contour lines around each Dirac point, when the energy is low, say, $E/t = 0.2$, the contour line is almost a circle, indicating that

the $E - \mathbf{k}$ relation is isotropic, which is characteristic of the relativistic Dirac equation. For larger energy, say $E/t = 0.6$, trigonal warping distortions occur,[51–54] leading to an anisotropic $E - \mathbf{k}$ relation bearing the hexagonal symmetry of a graphene lattice. The distortions become more dominant as the energy is increased further. Therefore, people usually concentrate on the energy levels in the low energy range, so that the results can be meaningfully compared with those from the relativistic neutrino billiards.
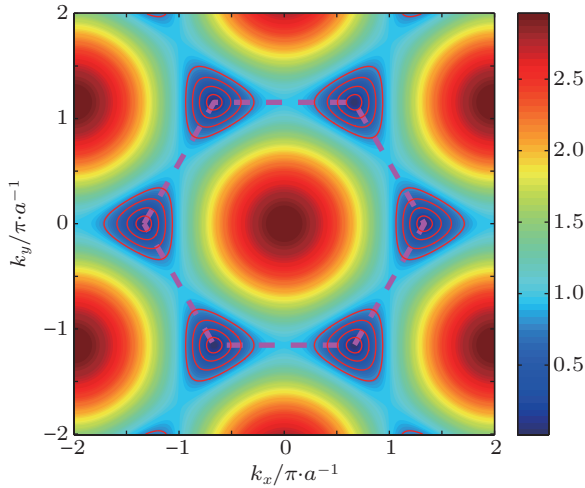
Fig. 3. Contour plot of energy in the momentum space for an infinite graphene flake. Here, $a = \sqrt{3}a_0 = 2.46$ Å is the lattice constant, and k_x is along the zigzag direction. The dashed line indicates the first Brillouin zone. The four sets of solid contour lines around each individual Dirac point are for $E/t = 0.2, 0.4, 0.6, 0.8$ (inside out), respectively. From Ref. [50].

3.2. Effects of disorder

The effects of disorder to the level spacing statistics has been considered in Refs. [27], [29], [55]–[58]. Libisch, Stampfer, and Burgdörfer[55] considered a rectangular phase-coherent graphene flake in the presence of disorder. The disorders they considered included edge roughness ΔW (see Figs. 4(a)–4(b)), short-range disorder n_D due to randomly distributed point defects in the interior, and long-range screened Coulomb distortion n_C due to charge deposition in either the substrate or the flake. The system has linear dimensions of 10–40 nm. In their calculation, a third nearest-neighbor tight-binding approximation is employed to correctly reproduce the graphene band structure.[59] The modified C–C bond length at the flake boundary is accounted for by increasing nearest-neighbor coupling to the outmost carbon atoms by 12% in accordance with recent *ab initio* density-functional calculations.[60] Then the spectrum of the graphene flake is determined by employing a Lanczos algorithm[61] giving the 500 eigenstates closest to the Fermi edge, and ensemble averages encompass typically 5000 disorder realizations. After unfolding the spectrum, they found for the ideal rectangular graphene dot a near-perfect Poisson distribution. By gradually increasing either the edge roughness or the defect concentra-

tion, the distribution smoothly evolves into a GOE statistic. Remarkably, for moderate values of the edge roughness amplitude $W = 0.4$ nm, a Schröinger and a graphene billiard of the same geometry display a markedly different level spacing statistics: while the Schröinger billiard has already reached the GOE limit, for the graphene the LSS still is closer to the Poisson limit, pointing to the unique spectral properties of graphene.
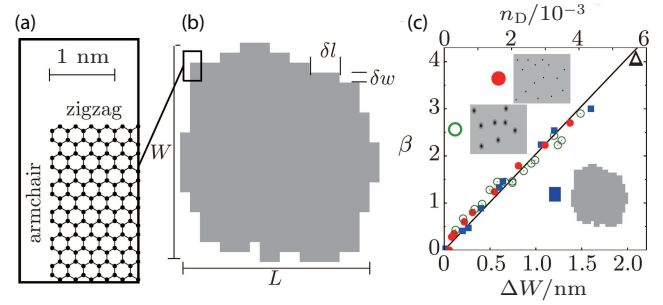
Fig. 4. (a) Rectangular segment of a graphene flake, vertical edge armchair, and horizontal edge zigzag terminated. (b) Approximately rectangular quantum dot with rough edges. (c) Dependence of parameter β for the transition from a Poisson to a GOE distribution on the edge roughness amplitude ΔW (squares), and the density of short-range (n_D, full circles) or of long-range ($n_C = 4n_D$, rescaled for demonstration purposes only, open circles) impurities. From Ref. [55].

The results are also fitted to the two-parameter Hasegawa distribution (8),[45] where a larger fitted parameter β indicates a better fit to the GOE distribution. They found $\alpha = 0.75$ to correctly reproduce the numerically obtained level spacing distributions for different values of both edge roughness as well as scatterers. A strong edge roughness of 2 nm (or impurity concentration $n_D = 5 \times 10^{-3}$, $n_C = 2 \times 10^{-2}$) is required to reach the chaotic limit, i.e., GOE statistics. Note that n_D and n_C are given in units of impurities per carbon atom, which should be within 1.8×10^{-3}, as estimated in Ref. [62].

By fitting with the Hasegawa distribution, they found a linear relation between β and the extent of disorder, e.g., between β and edge roughness $\beta \approx 2\Delta W$, and between β and the density of short-range scatterer $\beta \approx 0.7n_D$, as well as long-range defects $\beta \approx 0.2n_C$. This has been demonstrated in Fig. 4(c). This linear relation can be used to estimate the strength of the disorder in a graphene flake. For example, using the data in Ref. [27], they found the corresponding $\beta \approx 4$, indicating a disorder strength of $\Delta W \approx 2$ nm or $n_D \approx 5.5 \times 10^{-3}$.

Amanatidis and Evangelou[56] examined the disorder effects in graphene nanotubes. Their theoretical model considers only the nearest neighbor hopping energy, and the disorder (uniformly distributed randomness) is introduced to either onsite energies (the first term of Eq. (16)) or the nearest neighbor hopping energies (the second term of Eq. (16)). They found that the expected integrable Poisson statistics of the clean limit becomes GOE with level repulsion for weak

disorder. Moreover, their study of wide and short finite nanotube dots $W/L \gg 1$, which is the opposite limit from the usual nanotubes, confirms the presence of pseudodiffusive behavior even in the infinitesimally small disorder limit. In the opposite limit of narrow long cylinders resembling usual nanotubes $W/L \ll 1$, the corresponding level statistics is ballistic δ-function type, similar to that of the pure one-dimensional chain. For strong disorder, when the energy fluctuation is comparable to the hopping energy, the results for disordered carbon nanotubes suggest a return to Poisson statistics due to the onset of Anderson localization.[56] In a recent study, Amanatidis et al.[57] found that for weakly disordered graphene flakes with zigzag edges, the obtained level-spacing distribution for the first two positive energies in the Dirac region is neither chaotic (GOE) nor localized (Poisson), but similar to that at the critical point of the Anderson metal-insulator transition. The quantum transport in finite graphene can occur via critical edge states as in topological insulators.

Tan et al.[29] measured the conductance of the graphene nanoribbon quantum dot with a size of 500 nm by 60 nm at 20 mK, counted the resonance peaks at zero bias and did the level spacing statistics. The results suggested level repulsion and GOE statistics. They attributed the observation to the ripple type of disorders, which introduce random scatterings that mix different levels.

3.3. Effects of chaos

Regarding the effects of chaos on the level spacing statistics of graphene quantum dots, Ponomarenko et al.[27] reported on the electron transport in quantum dot devices carved entirely from graphene. At large sizes (> 100 nm), they behave as conventional single-electron transistors, exhibiting periodic Coulomb blockade peaks. For quantum dots smaller than 100 nanometers, the peaks become strongly nonperiodic, indicating a major contribution of quantum confinement. Random peak spacing and its statistics are well described by the theory of chaotic quantum billiards. Similar features have also been observed in a tunable graphene single electron transistor.[28]

In order to investigate more systematically the effect of chaos on the level spacing statistics of graphene billiards, in Refs. [50] and [63] the authors considered two billiard shapes that are commonly used in the study of level-spacing statistics, the Africa billiard[64] and one eighth of the Sinai billiard. Only the nearest neighbor hopping energy $t \approx 2.8$ eV[12] is considered. Matlab was used to calculate the eigenvalues. The Africa billiard contains 35542 atoms. The outline is determined by the equation $x + \mathrm{i}y = 64(z + 0.2z^2 + 0.2z^3 \mathrm{e}^{\mathrm{i}\pi/3})a$, where z is the unit circle in the complex plane, $a = \sqrt{3}a_0 = 2.46$ Å. The area of the billiard is $A = 934$ nm^2.

Figure 5 shows the band structure for a zigzag nanoribbon without (Fig. 5(a)) and with a magnetic field (Figs. 5(b)–5(d)). For a sufficiently strong magnetic field, the linear $E - \boldsymbol{k}$ relation, even for small energy, is violated, as Fig. 5(d) shows. Therefore, the parameters are chosen to stay in the regime where the linear $E - \boldsymbol{k}$ relation is preserved while the magnetic field is strong enough so that the magnetic effects are apparent enough. Three cases are considered: $\phi = 0$ (without magnetic field), $\phi = 1/8000\phi_0$ (weak magnetic field), and $\phi = 1/800\phi_0$ (strong magnetic field).[65]
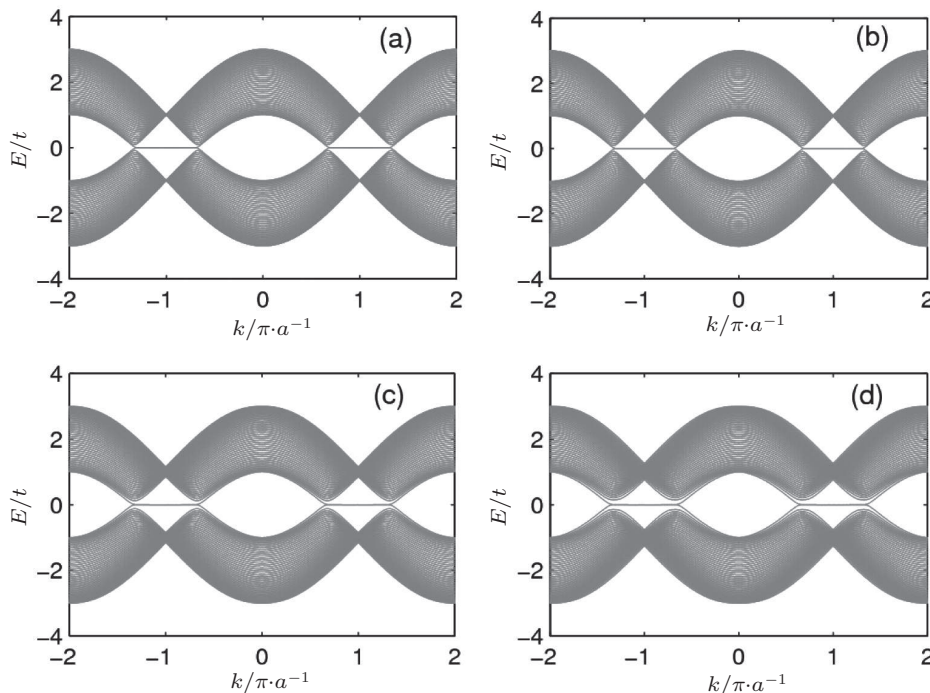
Fig. 5. Energy–momentum relation for graphene nano-ribbon with zigzag horizontal boundary. (a) $\phi = 0$; (b) $\phi = 1/8000\phi_0$; (c) $\phi = 1/800\phi_0$; (d) $\phi = 1/500\phi_0$. Each layer of the ribbon contains 100 atoms. From Ref. [50].

Results without magnetic field For the relativistic chaotic quantum billiard, the smoothed wavevector staircase function for positive eigenvalues is given by Eq. (15) with $\gamma = 0$[31]

$$\langle N(k)\rangle = Ak^2/4\pi + C_1 + \cdots, \tag{18}$$

where $C_1 = -1/12$ is a constant. For the chaotic graphene billiard, around a Dirac point $E = \hbar v_{\mathrm{F}} k$, where $v_{\mathrm{F}} = \sqrt{3}ta/2\hbar$ is the Fermi velocity, and $a = 2.46$ Å is the lattice constant. Thus

$$E = \sqrt{3}tak/2.$$

For the n-th energy level E_n, one has

$$k_n = \frac{2}{\sqrt{3}a} \cdot \frac{E_n}{t}.$$

Once the eigenenergy E_n is determined, the corresponding wave vector k_n can be obtained through the above relation. For the Africa graphene billiard, figure 6(a) shows, for eigenenergies in the range $0 < E_n/t < 0.4$, the wavevector staircase

function. The solid curve is given by

$$\langle N(k)\rangle = Ak^2/2\pi + C_1', \tag{19}$$

where $C_1' = 35$ is a fitting constant. Equation (19) differs from Eq. (18) in the leading 'Weyl' term by a factor of 2. This could be understood as follows. For a single Dirac point, one expects $\langle N(k)\rangle$ to follow Eq. (18). However, a finite graphene has two non-equivalent Dirac points, thus $\langle N(k)\rangle$ should be twice that given by Eq. (18), so the denominator becomes 2π (instead of 4π). The fitting constant C_1' is due to the edge states on the segments of the zigzag boundaries of the graphene billiard where their energies are all about zero. For a zigzag ribbon, the edge states exist for $E < E_{\mathrm{c}} = \hbar v_{\mathrm{F}}/L = \sqrt{3}ta/(2L)$, where L is the width of the ribbon.[66] The sizes of the graphene billiards are about $100a$, leading to $E_{\mathrm{c}} \simeq 0.01t$. The edge states are localized on segments of the zigzag boundaries. These states are essentially degenerate states, contributing to an artificial bias in the spectral staircase function for small energy values. Therefore, a minimum value of $2E_{\mathrm{c}} = 0.02t$ for E_n is set to exclude the edge states from consideration.
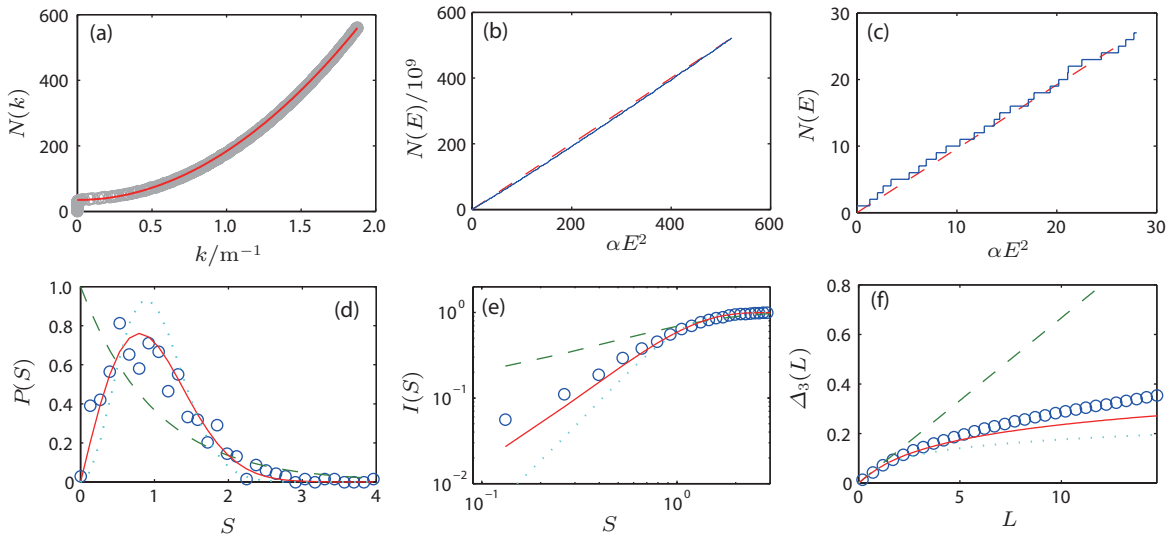
Fig. 6. Level-spacing statistics for the Africa billiard in the absence of a magnetic field ($\phi = 0$). (a) Wavevector staircase function $N(k)$ for eigenenergies $0 < E_n/t < 0.4$, where the number of energy levels is 560 (circles). The curve is $\langle N(k)\rangle = Ak^2/(2\pi) + 35$ [Eq. (19)]. (b) Spectral staircase function $N(E)$ versus αE^2 for $0.02 < E_n/t < 0.4$ with 522 levels, where α is the unfolding normalization constant. The dashed straight line is the averaged staircase function Eq. (20). (c) Magnification of part of panel (b) for $0.02 < E_n/t < 0.1$ with 28 levels. (d) Unfolded level-spacing distribution $P(S)$. (e) Cumulative unfolded level-spacing distribution $I(S)$. (f) Spectral rigidity Δ_3. In panels (d)–(f), numerical data are represented by open circles and the lines are theoretical predictions from the random matrix theory: dashed line for Poissonian, solid line for GOE, and dotted line for GUE statistics.[50]

Since $E = \hbar v_{\mathrm{F}} k$ for graphene billiards, the smoothed spectral staircase function is given by

$$\langle N(E)\rangle = \frac{AE^2}{2\pi\hbar^2 v_{\mathrm{F}}^2} + C_2 = \alpha E^2 + C_2, \tag{20}$$

where $\alpha = A/(2\pi\hbar^2 v_{\mathrm{F}}^2)$ is the unfolding normalization parameter and C_2 is now zero after setting $2E_{\mathrm{c}}$ for the minimum value of E_n. Figure 6(b) shows the spectral staircase function

of E_n for $0.02 < E_n/t < 0.4$, and figure 6(c) shows a magnification of part of Fig. 6(b) for eigenenergies in the range $0.02 < E/t < 0.1$. The dashed lines in these two panels are Eq. (20) with $C_2 = 0$. They agree well with the numerical results. The distribution of the unfolded level-spacing for the Africa graphene billiard is shown in Fig. 6(d), and the cumulative distribution is shown in Fig. 6(e). From the figures, it can be seen that the level-spacing follows the GOE statistics. Fig-

ure 6(f) shows the spectral rigidity for the calculated eigenenergies of the Africa billiard. This, together with Figs. 6(d) and 6(e), represents strong evidence that the level-spacing distribution in a chaotic graphene billiard in the relativistic quantum regime follows the GOE statistics. Similar plots have been obtained for one-eighth of the Sinai billiard with 37401 atoms and an area of $A = 1.607 \times 10^4 a^2 = 972$ nm^2, which also show GOE statistics.

The GOE statistics of unfolded level-spacing seem to be counterintuitive as one would expect that the graphene chaotic billiards should exhibit the same GUE level-spacing distribution as the neutrino billiard,[31] since they obey the same massless Dirac equation. However, since the graphene has two non-equivalent Dirac points (valleys), the time-reversal symmetry for the neutrino is actually the symplectic symmetry for graphene, which is the time-reversal symmetry in a single valley.[11] Thus the time-reversal symmetry breaking caused by the chirality in the neutrino billiards does not infer time-reversal symmetry breaking in graphene billiards. A detailed explanation for this is as follows. In graphene, quasiparticles in the vicinity of a Dirac point obey the same Dirac equation as for a neutrino, but the confinement to realize the billiard plays a different role. In particular, the abrupt edge termination in graphene billiard couples the two valleys in the momentum space. As a result, the wavefunctions for quasiparticles with wavevectors near the two Dirac points are no longer separable, rendering invalid the description of the two-component spinor Dirac equation for the whole system. A full set of equations taking into account the two nonequivalent Dirac points and the boundary conditions are thus necessary to describe the motions of the relativistic particle. Especially, the time-reversal symmetry is preserved,[11] suggesting that the system belongs to either the GOE or the GSE class. In this regard, the abrupt edge termination in a graphene billiard can be described by a step function in the form of an infinite potential at the edge. Since the range of the potential is short, the two valleys in the momentum space are coupled, which also breaks the sublattice symmetry. Since both the pseudospin valley symmetry and the sublattice symmetry are broken, Kramer's degeneracy and GSE statistics can be ruled out.[67] The resulting level-spacing statistics belong then to GOE. Similar effects have been noticed by Robnik and Berry that, in certain cases, although the system possesses neither time-reversal symmetry nor geometric symmetry (or other dynamical symmetries), it can be invariant under the combination of the two symmetries, and nontrivial representations can be found in which the Hamiltonian matrix elements are real, leading to GOE statistics (other than GUE).[68]

The results so far are for ideal chaotic graphene billiards. In experimental situations, a number of non-idealities can arise. To be experimentally observable, the GOE statistics should be robust even when these non-idealities are present. It is thus important to investigate the robustness of the level-spacing statistics of chaotic graphene billiards under various realistic considerations. In Refs. [50] and [63], the authors also considered non-ideal situations, such as interactions beyond the nearest neighbors, lattice orientation, effect of boundary bonds and staggered potentials caused by substrates, etc., and found that the GOE statistics are quite robust to these non-idealities.

Results with magnetic field   The presence of a magnetic field breaks the time-reversal symmetry of the graphene system[11] and, consequently, the level-spacing distribution belongs to the GUE class. This has been verified by the numerical results for both the Africa billiard and the one-eighth of the Sinai billiard with a uniform magnetic field $\phi = \phi_0/8000$.

For a stronger magnetic field, e.g., for $\phi = \phi_0/800$, the quantization of the energy levels to Landau levels becomes evident. The energy levels are clustered, leading to $\partial N/\partial E \to \infty$ at the Landau levels. The staircase counting function deviates markedly from the semiclassical predictions. The level spacing statistics for this case has not much meaning, but if one proceeds with the same procedures for the eigenenergies close to zero, the results of $P(S)$ and $I(S)$ show deviations from GUE, and are in fact closer to GOE. Intuitively, this can be understood by noting that the Landau levels "squeeze" the energy levels around them, resulting in smaller level-spacings and larger values of $P(S)$ for small S. At the same time, since the overall slope of the staircase counting function is unchanged, the squeezing of energy levels around the Landau levels tends to stretch the energy levels in between two successive Landau levels, yielding large level-spacings and larger values of $P(S)$ for large S. This stretching "pushes" the level-spacing distribution from GUE to GOE. Similar results have been observed in non-relativistic quantum chaotic billiards where the system is described by Schrödinger equation, in the energy range where the density of states is low and the Landau levels are apparent. The spectral rigidity, however, does not fall into any of the three known categories. This is due to the fact that the staircase function no longer follows the semiclassical prediction when the effects of the Landau levels cannot be neglected for a strong magnetic field.

For higher energy levels, e.g. $0.4 < E/t < 0.7$, where the Landau level is not apparent, the level-spacing statistics return to the GUE class again. Although in this energy range, trigonal warping becomes dominant (Fig. 3), which renders the theoretical description of the Dirac equation inappropriate, the energy levels can be accessible in experiments and thus relevant to graphene quantum-dot operations. In this region, $N(E_n)$ still depends hyperbolically on E_n, indicating a linear dependence between E_n and k_n. This is because in this energy range, the trigonal warping determines the scars (electron den-

sity patterns obtained from eigenstates) in the system, and restrains them to having line segments only in three directions, e.g., from the Dirac points to the origin.[20] Along these directions, the $E - k$ relation is approximately linear up to $E/t \sim 1$. This explains the hyperbolic relation between $N(E_n)$ and E_n even for high energies far away from the Dirac point.

The above observation of the GUE statistics for higher eigenenergies, from another aspect, corroborates the arguments that around the Dirac point, the energy level-spacing statistics are shifted "artificially" to GOE by the Landau levels. This could be important as the level-spacing can possibly be revealed in the peak spacings of the conductance in the corresponding quantum dots made from "open" billiards.[70]

Magnetic field effects in classical billiards have been studied in Refs. [71], [72], and [73], where it was found that for billiards with sufficiently smooth boundaries, such as the integrable elliptical billiard system, flyaway chaos can be induced by an intermediate magnetic field, but increasing the magnetic field further to the Landau regime can squeeze out the existence of this chaos.

3.4. Level spacing statistics for edge states

The level spacing statistics of only the edge states of graphene billiards has been discussed in Ref. [74]. The dot has the shape of a deformed disk, with a radius $R(\theta)$ depending on the angle of direction θ. The numerical calculations presented in the text use $R(\theta) = R_0 + 0.2R_0 \sin(\theta) + 0.05R_0 \sin(2\theta) - 0.025R_0 \sin(3\theta) + 0.02R_0 \sin(4\theta) - 0.01R_0 \sin(5\theta)$, with $R_0 = 160a \approx 40$ nm. In order to distinguish between edge and bulk states, for each eigenstate ψ they calculated the participation ratio[75,76]

$$p = \frac{(\sum_i |\psi(i)|^2)^2}{N \sum_i |\psi(i)|^4},$$

where the index i runs over atomic sites and N denotes the total number of atoms in the dot. The participation ratio p can be interpreted as the fraction of atoms occupied by an electron for a given energy level. Thus, $p \sim 1$ for extended states ($p \approx 0.3 - 0.4$ in quantum dots) and $p \ll 1$ for localized edge states ($p \approx 10^{-4} - 10^{-2}$). A state has been identified as an edge state if its participation ratio $p < 0.05$. The result does not change qualitatively if the threshold participation ratio is changed. In particular, the classification into the different types of level statistics does not depend on this threshold. In the case that the hopping energy for the second nearest neighbor $t' = 0$, the states with an energy smaller than the numerical precision have also been omitted.

Being localized, the edge states are expected to follow Poisson statistics, as noted in Ref. [19]. Surprisingly, as shown in Fig. 7, the level-spacing distributions for the electron-hole symmetric case $t' = 0$ follow the GOE statistics, and only for

broken electron-hole symmetry $t' = 0.1t$, do they exhibit a statistics close to Poisson.
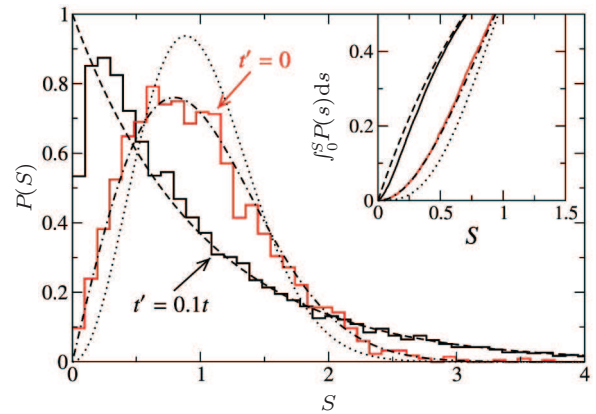
Fig. 7. Level-spacing distributions for quantum dots with smooth edges for $t' = 0$ (solid red curve) and $t' = 0.1t$ (solid black curve), together with the theoretical predictions for Poisson (dashed line), GOE (dashed-dotted line), and GUE (dotted line). The inset shows details of the integrated level spacing distribution for small level spacings S (same line colors and types as the main plot). The level distribution statistics has been obtained by averaging individual level distributions from 100 quantum dots similar to the type given in the text, with average radius $R_0 = 160a$. From Ref. [74].
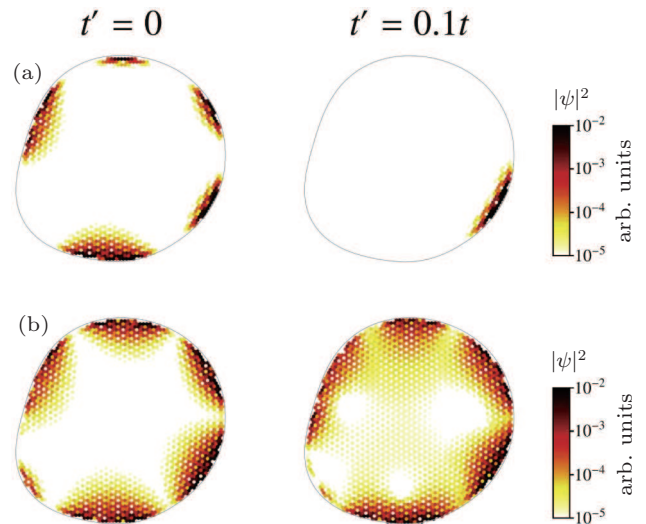
Fig. 8. Color plot of wavefunction density in a graphene quantum dot (shape as described in the text) for the electron–hole e–h symmetric case $t' = 0$ (left column) and for broken e–h symmetry $t' = 0.1t$ (right column) on the examples of a mode that is (a) strongly decaying and (b) slowly decaying into the bulk. Note that for presentation purposes, a rather small dot $R_0 = 30a$ has been chosen but the behavior does not change qualitatively for larger dots. From Ref. [74].

This striking difference in level statistics can be understood by the different nature of the wave functions. The graphene Hamiltonian exhibits a symmetry for $t' = 0$ that results in an equal occupation probability of sublattice A and B for every individual wave function.[66] Since the edge wave function at a certain type of zigzag edge is nonzero only on one sublattice, every eigenstate for $t' = 0$ must also occupy another part of the boundary of the opposite kind, as illustrated in Fig. 8. This leads to an artificial long-range coupling between edge states and thus to level repulsion, resulting finally

in GOE statistics. If this symmetry is broken, for example, by next-nearest-neighbor hopping, edge-state wave functions may be localized at a single edge only. Note that in the plot of Fig. 8, close to a boundary, the edge states occupy a single sublattice only. In order to avoid the oscillatory pattern on the lattice scale that inevitably arises when plotting both sublattices simultaneously, for every unit cell only the atom with the largest occupation probability is plotted.

3.5. Efforts to decouple the two valleys and search for GUE statistics in graphene billiards without magnetic fields

Since graphene has quasiparticles that mimic relativistic, massless Dirac fermions, it thus seems quite feasible, at first, to test the prediction of Berry and Mondragon for the GUE statistics of Dirac particles[31] by using classically chaotic graphene confinement systems. However, as graphene has two valleys, the corresponding quasiparticle view is then that graphene has two massless Dirac fermions which are coupled together by abrupt edge cuts or short range disorders. Therefore, a graphene billiard mimics a billiard that contains two massless Dirac fermions with certain interactions. The whole system, including the confinement and also the interaction between the two quasiparticles, preserves the time-reversal symmetry, therefore, the level spacing statistics of chaotic graphene billiards show those of GOE, as demonstrated in Section 3.3. Then the reasoning is that, if one can decouple the two quasiparticles so that they move independently, within a confinement that is also created with a mass term, could one get the GUE statistics?

Wurm *et al.*[19] addressed this question using a smooth varying mass term as the confinement. The mass term may originate from an effective staggered potential caused by possible edge magnetization of graphene flakes.[77,78] They considered an Africa billiard of 68169 carbon atoms using about 3000 energy levels in the range $[-0.5t, 0.5t]$. The mass term is given by $\sum m_i |i\rangle\langle i|$, which is positive (negative) if i belongs to sublattice A (B). For smooth mass confinement, the mass term is zero in the interior but nonzero within a distance $W = 4.5\sqrt{3}a$ of the boundary; it starts from zero at the inner border of this region and increases quadratically: $m(x, y) = \omega^2 [\delta(x, y) - W]^2/2$, where $\delta(x, y)$ is the distance to the boundary and $\omega = 0.15\sqrt{t}/a$ is a constant. While the lattice eventually terminates, the smooth varying confinement prevents the particles from feeling the rough boundary and thus suppresses the intervalley scattering. This preserves the valley symmetry, but breaks the sublattice symmetry, which also breaks the time-reversal symmetry in each valley.[19] If the two valleys are decoupled (no or weak intervalley scattering), the Hamiltonian consists of two degenerate blocks, each corresponding to a quasiparticle with unitary symmetry. However, the expected GUE level-spacing statistics have

not been observed. This was explained in that, although the mass term is relatively smooth, the system may still have some residual intervalley scattering, and the scattering time could be shorter than the relevant Heisenberg time scale for the level spacing, rendering the system to the GOE class.[19] These symmetry properties[11,79–81] are also related to pseudospin effects in the system, which could lead to the absence of backscattering[82,83] and the weak-localization or antilocalization phenomena,[67,84–88] and also to the universal conductance fluctuations of different universal classes.[19,89]

Rycerz[58] investigated the level spacing statistics of highly symmetric (triangular and hexagonal) graphene nanoflakes, considering armchair, zigzag, and Klein[90,91] boundaries. The advantage of these shapes is that the boundary is pure, it contains only one type of these boundaries, either armchair, or zigzag, or Klein; they are not mixed as in other cases. Without disorder, due to geometric symmetry, the energy levels are clustered and they do not fit in the random matrix ensembles. Adding disorder, attributed to the influence of substrate impurities (or ions),[92–95] will impose a transition of the level spacing statistics from Possionion-like to GOE distribution. The numerical results show that the orthogonal symmetry appears generically in closed graphene nanosystems. In a peculiar case of triangular nanoflakes with zigzag (or Klein) edges and smooth impurity potential, the unitary symmetry class seems to be the relevant one. A further study by Rycerz[96] investigating the effects of the strain fields, which can be regarded as a strain-induced gauge field, showed that if the zigzag triangular nanoflake is deformed such that all its geometric symmetries are broken, the spectral statistics seems to follow the GUE, while if a mirror symmetry is present, the spectral statistics follow the GOE.

4. Concluding remarks and discussion

In this short review, we have briefly summarized the results by Berry and Mondragon that the 2D massless Dirac particle, when confined in a finite region, breaks the time-reversal symmetry due to the infinite-mass confinement potential, rending GUE statistics of the level spacing distribution for chaotic billiards in the absence of a magnetic field. Graphene, a single-atom-layer of carbon atoms arranged in a honeycomb lattice, has low energy quasiparticles mimicking the 2D massless Dirac particle when neglecting the intervalley scattering. For an infinite graphene flake without disorder, the system preserves the pseudospin symmetry (the symmetry between A and B atoms) and also the symmetry between the two valleys. However, for finite graphene billiards, the above two symmetries are typically broken. The two valleys (or two quasiparticles) are coupled, and in terms of energy level distributions, without a magnetic field, the GOE statistics are prevalent.

The connection between the symmetry of the system and the random matrix ensembles of level spacing statistics lies in the matrix representations of the Hamiltonion.[3,97] For example, for a system that preserves time-reversal symmetry and neglecting spin, for any representation that has an orthogonal basis set, a T-invariant basis can be constructed, under which the Hamiltonian matrix is real symmetric.[3,98] In general, the Schrödinger equation of a spinless particle is time-reversal invariant if the Hamiltonian is a real matrix in the position representation.[3] If the classical dynamics are chaotic, it will introduce randomness into the real symmetric Hamiltonian matrix, leading to GOE for the LSS. However, if the time-reversal symmetry is broken and there are no other antiunitary symmetries (e.g., reflection together with TRS), without such restrictions, the Hamiltonian matrix is preserved by any unitary transformation. Although one can always find a representation in which the elements of the Hamiltonian matrix are all real, a general unrestricted unitary transformation will result in a complex Hamiltonian matrix. In addition, due to the randomness either caused by the nonregular boundary or the inner disorder, the matrix will be a random Hermitian matrix with complex elements. The resulting energy level statistics will then be GUE.

In this regard, since the tight-binding Hamiltonian of graphene billiard for the cases with short-range or long-range disorder, or with strain, or with mass term, insofar as there is no magnetic field, all these variations only add randomness to the Hamiltonian matrix, but the matrix elements are all real in the position representation. Therefore, the resulting Hamiltonian matrix is a real symmetric random matrix, preserving T and usually leading to GOE. However, as demonstrated in Refs. [99] and [100], even for a time-reversal invariant system, a subset of eigenstates can be identified if the system has an appropriate discrete symmetry, that this subset could present GUE behavior.

References

[1] Stöckmann H J 1999 *Quantum Chaos: An Introduction* (New York: Cambridge University Press)
[2] Gutzwiller M 1990 *Chaos in Classical and Quantum Mechanics* (Berlin: Springer)
[3] Haake F 2010 *Quantum Signatures of Chaos* (Springer)
[4] Bohigas G and Giannoni M J 1984 *Mathematical and Computational Methods in Nuclear Physics*, Lecture Notes in Physics, Vol. 209 (Berlin: Springer)
[5] Bohigas G, Giannoni M J and Schmit C 1984 *Phys. Rev. Lett.* **52** 1
[6] Berry M V 1985 *Proc. R. Soc. London A* **400** 229
[7] Weidenmüller H A and Mitchell G E 2009 *Rev. Mod. Phys.* **81** 539
[8] A requirement for the applicability of random-matrix theory is that the system possess no geometric symmetry.
[9] Stoffregen U, Stein J, Stöckmann H J, Kuś M and Haake F 1995 *Phys. Rev. Lett.* **74** 2666
[10] So P, Anlage S M, Ott E and Oerter R N 1995 *Phys. Rev. Lett.* **74** 2662
[11] Beenakker C W J 2008 *Rev. Mod. Phys.* **80** 1337
[12] Castro N A H, Guinea F, Peres N M R, Novoselov K S and Geim A K 2009 *Rev. Mod. Phys.* **81** 109
[13] Peres N M R 2010 *Rev. Mod. Phys.* **82** 2673
[14] Das Sarma S, Adam S, Hwang E H and Rossi E 2011 *Rev. Mod. Phys.* **83** 407
[15] Konig M, Wiedmann S, Brune C, Roth A, Buhmann H, Molenkamp L W, Qi X L and Zhang S C 2007 *Science* **318** 766
[16] Hsieh D, Qian D, Wray L, Xia Y, Hor Y S, Cava R J and Hasan M Z 2008 *Nature* **452** 970
[17] Hasan M Z and Kane C L 2010 *Rev. Mod. Phys.* **82** 3045
[18] Qi X L and Zhang S C 2011 *Rev. Mod. Phys.* **83** 1057
[19] Wurm J, Rycerz A, Adagideli I, Wimmer M, Richter K and Baranger H U 2009 *Phys. Rev. Lett.* **102** 056806
[20] Huang L, Lai Y C, Ferry D K, Goodnick S M and Akis R 2009 *Phys. Rev. Lett.* **103** 054101
[21] Xu H Y, Huang L, Lai Y C and Grebogi C 2013 *Phys. Rev. Lett.* **110** 064102
[22] Yang R, Huang L, Lai Y C and Grebogi C 2011 *Europhys. Lett.* **94** 40004
[23] Ying L, Huang L, Lai Y C and Grebogi C 2012 *Phys. Rev. B* **85** 245448
[24] Yang R, Huang L, Lai Y C and Pecora L M 2012 *Appl. Phys. Lett.* **100** 093105
[25] Yang R, Huang L, Lai Y C, Grebogi C and Pecora L M 2013 *Chaos* **23** 013125
[26] Miao F, Wijeratne S, Zhang Y, Coskun U C, Bao W and Lau C N 2007 *Science* **317** 1530
[27] Ponomarenko L A, Schedin F, Katsnelson M I, Yang R, Hill E W, Novoselov K S and Geim A K 2008 *Science* **320** 356
[28] Stampfer C, Schurtenberger E, Molitor F, Güttinger J, Ihn T and Ensslin K 2008 *Nano Lett.* **8** 2378
[29] Tan C L, Tan Z B, Ma L, Chen J, Yang F, Qu F M, Liu G T, Yang H F, Yang C L and Lü L 2009 *Acta Phys. Sin.* **58** 5726 (in Chinese)
[30] Chen M, Fu Z G, Peng J P, Zheng F, Zhang H M, Feng X, Chang C Z, He K, Wang L, Zhang P, Ma X and Xue Q K 2013 arXiv:1312.4757v1 [cond-mat.mes-hall]
[31] Berry M V and Mondragon R J 1987 *Proc. R. Soc. London, Ser. A* **412** 53
[32] Neutrinos have a minuscule, but nonzero mass. See Karagiorgi G, Aguilar-Arevalo A, Conrad J M, Shaevitz M H, Whisnant K, Sorel M and Barger V 2007 *Phys. Rev. D* **75** 013011
[33] Phatak S C, Pal S and Biswas D 1995 *Phys. Rev. E* **52** 1333
[34] Novoselov K S, Geim A K, Morozov S V, Jiang D, Zhang Y, Dubonos S V, Grigorieva I V and Firsov A A 2004 *Science* **306** 666
[35] Akhmerov A R and Beenakker C W J 2007 *Phys. Rev. Lett.* **98** 157003
[36] Xiao D, Yao W and Niu Q 2007 *Phys. Rev. Lett.* **99** 236809
[37] Garcia-Pomar J L, Cortijo A and Nieto-Vesperinas M 2008 *Phys. Rev. Lett.* **100** 236801
[38] Berry M V and Tabor M 1977 *Proc. Roy. Soc. London, Ser. A* **356** 375
[39] Mehta M L 1967 *Random Matrices* (New York: Academic)
[40] Bohr A and Mottelson B R 1969 *Nuclear Structure*, Vol. 1 (New York: Benjamin) Appendix 2C, pp. 294–301
[41] Here we do not consider GSE since it is irrelevant to our studies.
[42] Dyson F J and Mehta M L 1963 *J. Math. Phys.* **4** 701
[43] Bohigas O and Giannoni M J 1975 *Ann. Phys.* **89** 393
[44] Liu B, Zhang G C, Ding L, Dai J H and Zhang H J 1999 *Phys. Lett. A* **260** 406
[45] Hasegawa H, Mikeska H J and Frahm H 1988 *Phys. Rev. A* **38** 395
[46] Li B W, Robnik M and Hu B 1998 *Phys. Rev. E* **57** 4095
[47] Ni X, Huang L, Ying L and Lai Y C 2013 *Phys. Rev. B* **87** 224304
[48] Ni X, Huang L, Lai Y C and Grebogi C 2012 *Phys. Rev. E* **86** 016702
[49] Ni X, Huang L, Lai Y C and Pecora L M 2012 *Europhys. Lett.* **98** 50007
[50] Huang L, Lai Y C and Grebogi C 2011 *Chaos* **21** 013102
[51] Saito R, Dresselhaus G and Dresselhaus M S 2000 *Phys. Rev. B* **61** 2981
[52] Rycerz A, Tworzydło J and Beenakker C W J 2007 *Nat. Phys.* **3** 172
[53] Cheianov V V, Fal'ko V and Altshuler B L 2007 *Science* **315** 1252
[54] Garcia-Pomar J L, Cortijo A and Nieto-Vesperinas M 2008 *Phys. Rev. Lett.* **100** 236801
[55] Libisch F, Stampfer C and Burgdörfer J 2009 *Phys. Rev. B* **79** 115423
[56] Amanatidis I and Evangelou S N 2009 *Phys. Rev. B* **79** 205420
[57] Amanatidis H, Kleftogiannis I, Katsanos D E and Evangelou S N 2013 arXiv:1302.2470 [cond-mat.dis-nn]
[58] Rycerz A 2012 *Phys. Rev. B* **85** 245424
[59] Reich S, Maultzsch J, Thomsen C and Ordejon P 2002 *Phys. Rev. B* **66** 035412
[60] Son Y W, Cohen M L and Louie S G 2006 *Phys. Rev. Lett.* **97** 216803

[61] Lanczos C 1950 *J. Res. Natl. Bur. Stand.* **45** 255

[62] Chen J H, Jang C, Adam S, Fuhrer M S, Williams E D and Ishigami M 2008 *Nat. Phys.* **4** 377

[63] Huang L, Lai Y C and Grebogi C 2010 *Phys. Rev. E* **81** 055203

[64] Berry M V and Robnik M 1986 *J. Phys. A: Math. Gen.* **19** 649

[65] The magnetic field can be scaled down for larger confinements to yield similar effects.

[66] Brey L and Fertig H A 2006 *Phys. Rev. B* **73** 235411

[67] Suzuura H and Ando T 2002 *Phys. Rev. Lett.* **89** 266603

[68] Robnik M and Berry M V 1986 *J. Phys. A: Math. Gen.* **19** 669

[69] Robnik M 1986 *Quantum Chaos and Statistical Nuclear Physics*, Lecture Notes in Physcs, Vol. **263** (Berlin: Springer-Verlag)

[70] Alhassid Y and Lewenkopf C H 1995 *Phys. Rev. Lett.* **75** 3922

[71] Robnik M and Berry M V 1985 *J. Phys. A* **18** 1361

[72] Robnik M 1986 *Nonlinear Phenomena and Chaos*, Malvern Physics Series (Bristol: Adam-Hilger)

[73] Robnik M 1986 *J. Phys. A* **19** 3619

[74] Wimmer M, Akhmerov A R and Guinea F 2010 *Phys. Rev. B* **82** 045409

[75] Bell R J and Dean P 1970 *Discuss. Faraday Soc.* **50** 55

[76] Bell R J 1972 *Rep. Prog. Phys.* **35** 1315

[77] Fujita M, Wakabayashi K, Nakada K and Kusakabe K 1996 *J. Phys. Soc. Jpn.* **65** 1920

[78] Wimmer M, Adagideli I, Berber S and Tománek D and Richter K 2008 *Phys. Rev. Lett.* **100** 177207

[79] Nomura K, Koshino M and Ryu S 2007 *Phys. Rev. Lett.* **99** 146806

[80] Ryu S, Mudry C, Obuse H and Furusaki A 2007 *Phys. Rev. Lett.* **99** 116601

[81] Ostrovsky P M, Gornyi I V and Mirlin A D 2007 *Phys. Rev. Lett.* **98** 256801

[82] Bena C 2008 *Phys. Rev. Lett.* **100** 076601

[83] Brihuega I, Mallet P, Bena C, Bose S, Michaelis C, Vitali L, Varchon F, Magaud L, Kern K and Veuillen J Y 2008 *Phys. Rev. Lett.* **101** 206802

[84] Ando T, Nakanishi T and Saito R 1998 *J. Phys. Soc. Jpn.* **67** 2857

[85] Morozov S V, Novoselov K S, Katsnelson M I, Schedin F, Ponomarenko L A, Jiang D and Geim A K 2006 *Phys. Rev. Lett.* **97** 016801

[86] McCann E, Kechedzhi K, Fal'ko V I, Suzuura H, Ando T and Altshuler B L 2006 *Phys. Rev. Lett.* **97** 146805

[87] Morpurgo A F and Guinea F 2006 *Phys. Rev. Lett.* **97** 196804

[88] Wu X, Li X, Song Z, Berger C and de Heer W A 2007 *Phys. Rev. Lett.* **98** 136801

[89] Kharitonov M Y and Efetov K B 2008 *Phys. Rev. B* **78** 033404

[90] Klein D J 1994 *Chem. Phys. Lett.* **217** 261

[91] Wakabayashi K, Okada S, Tomita R, Fujimoto S and Natsume Y 2010 *J. Phys. Soc. Jpn.* **79** 034706

[92] Lewenkopf C H, Mucciolo E R, Castro Neto A H 2008 *Phys. Rev. B* **77** 081410

[93] Mucciolo E R, Castro Neto A H and Lewenkopf C H 2009 *Phys. Rev. B* **79** 075407

[94] Carmier P and Ullmo D 2008 *Phys. Rev. B* **77** 245413

[95] Carmier P, Lewenkopf C and Ullmo D 2010 *Phys. Rev. B* **81** 241406

[96] Rycerz A 2013 *Phys. Rev. B* **87** 195431

[97] Ergün G 2012 *Computational Complexity* **2012** 2549

[98] It should be noted that the representation here is different than the energy representation, in which the Hamiltonian is diagonalized and is real.

[99] Leyvraz F, Schmit C and Seligman T H 1996 *J. Phys. A: Math. Gen.* **29** L575

[100] Dembowski C, Gräf H D, Heine A, Rehfeld H, Richter A and Schmit C 2000 *Phys. Rev. E* **62** R4516